Anisotropic emission and photon-recycling in strain-balanced quantum well solar cells

C. Cabrera, J. Rimada, L. Hernandez, James P Connolly, A. Enciso, D. Contreras-Solorio

Anisotropic Emission and Photon-recycling in Strain-Balanced Quantum Well Solar Cells

C. I. Cabrera[1], J. C. Rimada[2], L. Hernandez[3] , J.P. Connolly[4] A. Enciso[5] and D. A Contreras-Solorio[5]

[1] Department of Physics, University of Pinar del Río, Martí 270, 20100 Pinar del Río, Cuba.

[2] Solar cell laboratory, Institute of Materials Science and Technology (IMRE), University of Havana, Zapata y G, 10400 La Habana, Cuba.

[3] Faculty of Physics, University of Havana, Colina Universitaria. 10400 La Habana, Cuba.

[4]Nanophotonics Technology Center, Universidad Politécnica de Valencia, 46022 Valencia, Spain.

[5] Academic Unit of Physics, Autonomous University of Zacatecas, Czda. Solidaridad y Paseo La Bufa S/N, 98060 Zacatecas, Zac., México.

PACS: 85.35.Be; 62.20.-x; 68.65.Fg; 73.21.Fg; 73.63.Hs; 84.60.Jt; 85.30.De; 85.35.Be

Keywords: Quantum well; Strain in solids; Solar cell; Conversion efficiency; Modelling.

Abstract. Strain-balanced quantum well solar cells (SB-QWSC) extend the photon absorption edge beyond that of bulk GaAs by incorporation of quantum wells in the i-region of a p–i–n device. Anisotropy arises from a splitting of the valence band due to compressive strain in the quantum wells, suppressing a transition which contributes to emission from the edge of the quantum wells. We have studied both the emission light polarized in the plane perpendicular (TM) to the quantum well which couples exclusively to the light hole transition and the emission polarized in the plane of the quantum wells (TE) which couples mainly to the heavy hole transition. It was found that the spontaneous emission rates TM and TE increase when the quantum wells are deeper. The addition of a distributed Bragg reflector (DBR) can substantially increase the photocurrent while decreasing the radiative recombination current. We have examined the impact of the photon recycling effect on SB-QWSC performance. We have optimized SB-QWSC design to achieve single junction efficiencies above 30%.

I. Introduction

The strain-balanced quantum well solar cell (SB-QWSC) is a GaAs p-i-n solar cell with quantum well (QW) layers incorporated into the i-region with InGaAs as well material and GaAsP as barrier material. The compressive strain in the InGaAs QW is matched by tensile strain in GaAsP barriers, overcoming the lattice-mismatch limitation. Using this strain-balancing technique, more than 65 quantum well layers have been grown without dislocations [1, 2]. The purpose of this design is to improve the spectral response of the cell in the energy region below the absorption edge of host material, in order to gain an extra photocurrent and therefore an increment in the short-circuit current. Under solar radiation, a drop in open circuit voltage (V_{oc}) of a SB-QWSC is avoided, due to the inclusion of GaAsP with a higher bandgap than GaAs. This way the addition of short-circuit current (J_{sc}) from the quantum wells leads to an increase of the solar cell conversion efficiency. Photo-

generated carriers can escape from the quantum wells with near unity efficiency via a thermally-assisted tunneling process due to the presence of the built-in electric field in the intrinsic region. SB-QWSC can achieve optimal band-gaps for the highest single-junction efficiencies due to the tunability of the quantum well thickness and composition.
The GaAsP and InGaAs layer widths were chosen to ensure the average lattice parameter across the i-region was equal to that of GaAs. Elastic constants were considered to evaluate the tensile and compressive strain in GaAsP and InGaAs layers. Thus, if L_B is the barrier thickness, L_W is the well thickness, $a_{GaAs_{1-y}P_y}$ and $a_{In_xGa_{1-x}As}$ are the respective well and barrier lattice constants; we define

$$a_{GaAs} \equiv \langle a \rangle = \frac{L_B a_{GaAs_{1-y}P_y} + L_W a_{In_xGa_{1-x}As}}{L_B + L_W} \tag{1}$$

Biaxial strain can only be achieved on the nano-scale, giving nano-structured solar cells a fundamental advantage over bulk semiconductor solar cells. The changes in the band structure of the layer under strain have significant effects on the SB-QWSC. The growth of strained GaAsP and InGaAs layers allows a wider choice of P and In compositions to fit the energy levels in the quantum wells. Thus, the balanced strain between GaAsP and InGaAs layers is also designed as an extra parameter to tailor the layer materials and the SB-QWSC performance.

The total strain in the layer may be resolved into a hydrostatic component and an axial component. For unstrained bulk material, the heavy hole (*hh*) and light hole (*lh*) bands at the top of the valence band are degenerated at the Brillouin zone centre. The hydrostatic component of strain acts on the band edges, thereby changing the band gaps. However, it is the axial strain component, acting on degenerate bands such as in the valence bands, in which the axial component lifts the degeneracy that exists for the heavy-hole and light-hole bands at the band edge (Γ point). Under compressive strain, bottom energy of the conduction band is displaced to higher energy and the valence band splits, with the *lh* band moving further from the conduction. On the contrary, under tensile strain the GaAsP band gap is reduced and the highest valence band is the light hole band. Consequently, when the In an P compositions are varied, the strains in the barrier and well layers modify absorption threshold in both layers. This behavior was demonstrated in previous work [3].

Therefore, compressive strain results in lower thermal occupancy of the *lh* band relative to the *hh* band, and radiative transitions from the conduction to the *hh* band are favored over those to the *lh* band. If the splitting becomes greater than a few ~k_BT, *lh* transitions could be suppressed almost entirely [4, 5]. In order to examine this behavior, the anisotropic radiative recombination and gain, as consequence of the strain in the quantum wells, is investigated in this paper in order to determinate their influence in the SB-QWSC performance.

As a result of the dislocation-free material, the radiative recombination dominates in SB-QWSCs at high current levels. This makes possible the exploitation of radiative recycling by mean of the growth of distributed Bragg reflectors between the active region and the substrate of the cell which it has been possible to enhance SB-QWSC [6].

The observed rise in solar cell efficiency due to distributed Bragg reflectors (DBRs) is product of the reflection of photons back into the cell of photons (which would otherwise have been absorbed in the substrate) leading to photon recycling, that results when photons emitted by carrier

recombination are reabsorbed in the same device. The photon recycling effect can be observed as an increase in the quantum well absorption.

We will discuss the theoretical background to radiative recombination, gain, photon recycling and then present the results of simulations of the SB-QWSC that it takes account of DBR and anisotropic effects. We calculated quantum and conversion efficiencies and observed an increment in the SB-QWSC performance, particularly under solar concentration.

II. Anisotropic radiative emission and gain

In previous paper [3], it was shown that high SB-QWSC performance was achieved for 3% In composition. Moreover, for SB-QWSC with deeper quantum wells (higher indium fraction) the efficiency falls. However, the radiative recombination current could be suppressed in SB-QWSC devices with deep QWs relative to the prediction of the generalized Planck formula assuming isotropic emission. This effect was not considered in reference [3] but it will be taken into account in the present work.

Following reference [4,5], emission can be defined as TE, which is polarized in the plane of the QWs, and TM, which is polarized perpendicular to the plane of the QWs. It is therefore possible for TE-polarized light to be emitted either out of the face or the edge of the QWs, whereas TM-polarized light can only be emitted out of the edge of the QWs, as shown in Fig. 1. The *hh* transition couples solely to TE-polarized emission, and the *lh* band couples predominantly to TM-polarized emission with a minor TE-polarized contribution.

The spontaneous emission rates, R_{spon}, were calculated by ab-initio methods [7], where the transition from bulk to quantum wells structures was carried out by converting the 3D density of states to the 2D density states. To compute TE and TM emissions out of the faces and edges of a quantum well, it was considered that when the In and P compositions and their layer widths are varied, such that the condition given by Eq. (1) is satisfied, the generated strain modifies the spontaneous emission rate. The emission spectrum from a solar cell depends on the absorption coefficient and the carrier density through the quasi-Fermi-level separation, ΔE_f. To model the emission from either sample at a given generated strain we first calculated the absorption coefficient using a quantum-mechanical model. We solved for the energy levels of the strain-balanced QW within the envelope function approximation and then calculated the absorption coefficient using Fermi's golden rule. In order to determine the QW energy levels in the *hh* and *lh* bands under varying compressive strain a 4x4 $k \cdot p$ Kohn-Luttinger Hamiltonian was used [3]. Furthermore, valence band structure for holes in the quantum well was calculated using a 4x4 *k.p* Hamiltonian model. The ΔE_f values for the AM1.5 solar spectrum [8] were computed for a more general method to the one reported by Tsiu et al [9].

We assumed that the number of photogenerated carrier pairs is equal to the total emitted photo flux. In the absence of any photon density, the emission rate is the spontaneous emission rate, provided an electron is present in the state $\vec{k}$ and a hole is present in the same state $\vec{k}$ in the valence band. The rate depends on the occupation probability functions for electrons, f_e, and holes, f_h, with the same *k*-value. The occupation probability function for electrons and holes depends on the corresponded quasi-Fermi level. The spontaneous emission rate expression for quantum well structures is obtained be integration over all possible electronic state:

$$R_{spon} = \int d(\mathrm{h}\omega)\, \mathrm{A}\mathrm{h}\omega \sum_{n,m} \left[\begin{array}{l} \int \frac{d^2k}{(2\pi)^2} \left| \hat{a} \cdot \vec{p}_{if} \right|^2 \delta\left(E_n^e\left(\vec{k}\right) - E_m^h\left(\vec{k}\right) - \mathrm{h}\omega \right) \times \\ f_e\left(E_n^e\left(\vec{k}\right)\right) f_h\left(E_m^h\left(\vec{k}\right)\right) \end{array} \right] \tag{2}$$

The integral over $d(\mathrm{h}\omega)$ is to find the rate for all photon emitted and the integration over d^2k is to get the rate for all the occupied electron and hole subband state.

Equation (2) summarizes the discrete energy states of the electrons (index *n*) and the heavy holes (index *m*) in the well. $E_n^e\left(\vec{k}\right)$ and $E_m^h\left(\vec{k}\right)$ denote the QW subbands of the electrons and heavy holes and δ denotes the Dirac delta function. The factor $\mathrm{A} = 2q^2 n_r \big/ \left(m_0^2 c^3 \mathrm{h}^2\right)$ is a material dependent constant, where h is the reduced Planck constant, n_r is the refractive index of the well material, m_0 is the free electron mass, q is the electron charge and c is the speed of light. The first term inside the element $\left|\hat{a} \cdot \vec{p}_{if}\right|$ represents the polarization unit vector, $\hat{a}$, while the second term represents the momentum matrix element, $\vec{p}_{if}$. The spontaneous emission rate of the QWs was calculated using the above formula.

In a semiconductor in nonequilibrium condition, the total electron concentration *n* and the total hole concentration *p* are described to be the respectively electron and hole quasi-Fermi levels. If detailed balance is applied when each photons produce one electron-hole pair and all recombination events produce one photon, the electrons and hole quasi-Fermi levels in the quantum well structure were calculated by solving the following equation systems:

$$\begin{aligned} n\left(E_{F_e}\right) &= p\left(E_{F_h}\right) \\ \Delta E_f &= E_{F_e} - E_{F_h} \end{aligned} \tag{3}$$

where ΔE_f is the quasi-Fermi level separation.

Determining ΔE_f is essentially a matter of normalizing the emission spectrum to the generation rate. If detailed balance applies, the number of photogenerated carrier pairs is equal to the total emitted photon flux, and the gain (*G*) is defined as the number of photogenerated carrier pairs per unit area and time:

$$G = \int_0^\infty \int G(\lambda, z)\, dz\, d\lambda = \int_0^\infty L(\mathrm{h}\omega)\, d(\mathrm{h}\omega) \tag{4}$$

where $G(\lambda, z)$ is the electron-hole pair generation rate at a z depth from the surface in the grown direction and is given be the expression:

$$G(\lambda, z) = \left[1 - R(\lambda)\right] \alpha(\lambda, z) F(\lambda) \exp\left[-\int_0^z \alpha(\lambda, z')\, dz' \right] \tag{5}$$

where $R(\lambda)$ is the surface reflectivity spectrum of the antireflection layer (ARC), $F(\lambda)$ is the AM1.5 solar spectrum and $\alpha(\lambda, z)$ is the absorption coefficient to a z depth from the surface. The exponential factor is due to the attenuation of light in the layers between the surface of the cell and the depletion layer. The layers considered in our calculus are antireflection layer, emitter layer, and space-charge region from to the emitter layer (see figure 2).

The emitted flux density $L(\mathrm{h}\omega)$, of photons of energy $\mathrm{h}\omega$, is given by:

$$L(\mathrm{h}\omega) = \frac{2n_r^2}{h^3 c^2} \frac{\alpha(\mathrm{h}\omega)(\mathrm{h}\omega)^2}{e^{\frac{\mathrm{h}\omega - \Delta E_f}{k_B T}} - 1} \tag{6}$$

At low enough carrier density, where ΔE_f is much smaller than the effective band gap, the Boltzmann approximation is used, and Eq. (6) is simplified, then the dependence on ΔE_f is an explicit function. From Eq. (4) and Eq. (6), we found:

$$\Delta E_f = -k_B T \ln\left[\frac{1}{G}\int_0^{\infty} \frac{2{n_r}^2}{(2\pi\mathrm{h})^3 c^2} \alpha(\mathrm{h}\omega)(\mathrm{h}\omega)^2 e^{-\frac{\mathrm{h}\omega}{k_B T}} d(\mathrm{h}\omega)\right] \tag{7}$$

The total electron concentration is calculated by:

$$n = \int_{E_{w_e}}^{E_{b_e}} g_e^{QW}(E) f_e(E) dE + \int_{E_{b_e}}^{\infty} g_e^{Bulk}(E) f_e(E) dE \tag{8}$$

where E_{w_e} and E_{b_e} are the conduction valence band edge energy for quantum well and barrier material respectively, g_e^{QW} is the electron quantum well density of states and g_e^{Bulk} is the electron bulk density of states. To calculate the total hole concentration we proceed in a similar way. Then the equation system (3) may be solved and the quasi-Fermi level is determined. To compute the spontaneous emission rate from QW region, the expression (2) was used.

Figure 3 shows TE and TM spontaneous emission rates and its relation as a function of In fraction. The broken lines are due to the emergence of QW energy levels, e_2-hh_2 and e_2-lh_2 transitions, when the well depth increases. It can be seen that increasing In fraction, the QWs are under higher compressive strain, resulting in that radiative transitions from the conduction band to *hh* band (TE) are favored over those to *lh* band (TM). However, both polarized emissions increase with well depth, showing that biaxial compressive strain does not suppresses a mode of radiative recombination in the plane of the QWs, although certainly the TM/TE relation diminishes. So that, increasing the In composition leads to larger radiative recombination that increases the recombination dark current. In figure 4, spontaneous emission rates and gain are plotted as a function of In fraction. The spontaneous emission rates in QWs have already been displayed in a previous figure but are repeated here together to *G* to emphasize the huge difference between their values. From these results it follows that the generation of electron-hole pairs in the QWs is much higher than the radiative recombination, and if to these is added the existence of transverse electric field in the depletion region, which favors thermally assisted tunneling, then the carriers escape from the QWs with unity efficiency.

III. Photon-recycling

A DBR is a region consisting of layers of alternating refractive indices optimized for a specific wavelength such that each layer is a quarter wavelength thick. As a result, partial reflections from each interface interfere constructively and the reflectivity is high over a narrow wavelength band. Photon-recycling is the generation of an electron-hole pair via the absorption of a photon emitted elsewhere in the cell. The increased absorption is due to the reflection of incident solar radiation which has not been absorbed on its first pass through the cell and may then be reabsorbed on its second pass. It is equivalent to say that a DBR doubles the optical path length of a SB-QWSC without altering the length over which minority carriers must travel. The photons emitted by recombination into quantum wells were also considered. The net solar incident radiation flow on front surface of a solar cell was modeled as a Fabry-Perot cavity. We calculated the contribution of the multiple internal reflections inside the device and, so that the new AM1.5 solar spectrum $F_{net}(\lambda)$ is given by:

$$F_{net}(\lambda) = F(\lambda)\left[1+\frac{r_B\left(r_A+e^{\alpha_T^*}\right)}{e^{2\alpha_T^*}-r_B r_A}\right] \qquad (9)$$

$$\alpha_T^* = \sum_j \alpha_j(\lambda) l_j$$

Where $\alpha_j(\lambda)$ are the absorption coefficients of each layer of Fabry-Perot cavity structure, where it was taken into account the exciton effect in the quantum well, l_j are their widths and r_A, r_B are the internal reflectivity from the front and back surface of the cell, respectively.

The photocurrent J_{PH} is calculated from the total quantum efficiency (QE_{TOTAL}) of the cell:

$$J_{PH} = q\int_{\lambda_1}^{\lambda_2} F(\lambda)\left[1+\frac{r_B\left(r_A+e^{\alpha_T^*}\right)}{e^{2\alpha_T^*}-r_B r_A}\right] QE_{TOTAL}(\lambda)\,d\lambda \qquad (10)$$

where $\lambda_1 = 400\text{nm}$ and λ_2 is the effective absorption threshold determined by the fundamental electron and hole confinement states.

The p-region and n-region contribution to QE_{TOTAL} was classically evaluated solving the carrier transport equations at room temperature within the minority carrier and depletion approximations [10]. The contribution of photo-generated carriers in the intrinsic region to QE_{TOTAL} values is calculated by the expression [11]:

$$QE_i(\lambda) = \left[1-R(\lambda)\right]\exp\left\{-\sum_{j=1}^{3}\alpha_j z_j\right\}\times\left[1-\exp\left(-\alpha_B W - N_W\alpha_W^*\right)\right] \qquad (11)$$

where $R(\lambda)$ is again the surface reflectivity spectrum of ARC. The first exponential factor is due to the attenuation of light in the layers between the surface of the cell and the depletion layer (see figure 1). On the other hand, α_j and z_j are the absorption coefficient and the width of these precedent layers, respectively, α_B is the absorption coefficient of the bulk barrier material, and α_W^* is the dimensionless quantum well absorption coefficient, used for energies below the barrier band gap. Following Bastard [12], we calculate the density of states for the single quantum well within the

envelope function approximation. The dimensionless quantum well absorption coefficient can be calculated as follows:

$$\alpha_W^* = \alpha_W \Lambda \tag{12}$$

$$\alpha_W(E) = \sum_{n,m} \alpha_{e_n - hh_m}(E) + \sum_{n,m} \alpha_{e_n - lh_m}(E) \tag{13}$$

where α_W is the well absorption coefficient and Λ is the ''quantum thickness of the heterostructure'' which represents the width of the region containing the QW system, $\sum_{n.m} \alpha_{e_n - hh_m}(E)$ and $\sum_{n,m} \alpha_{e_n - lh_m}(E)$ are sums over well states *n* and *m*, which numbers depend on the quantum wells width and depth, $\alpha_{e_n - hh_m}(E)$ and $\alpha_{e_n - lh_m}(E)$ are the absorption coefficients due to electron-heavy hole and electron-light hole transitions to conduction band, respectively, which considered the exciton absorption to match accurately with experimental data in the long wavelength region.

The quantum well absorption coefficients $\alpha_{e_n\text{-}hh_m}(E)$ was computed by Fermi's Golden rule:

$$\alpha_{e_n\text{-}hh_m}(E) = \frac{\mathrm{B}E_p}{\Lambda E}\left|\left\langle \psi_{e_n} \middle| \psi_{hh_m} \right\rangle\right|^2 \left[\begin{array}{l} \dfrac{m^*_{e-hh}}{\mathrm{h}^2}\Theta\left(E - E_{g_w} - E_{e_n} - E_{hh_m}\right) \\ + \dfrac{4}{a_{ex}^2}\delta\left(E - E_{g_w} - E_{e_n} - E_{hh_m} + E^B_{e_n, hh_m}\right) \end{array} \right] \tag{14}$$

The formula summarizes the discrete energy states of the electrons (index *n*) and the heavy holes (index *m*) in the well. E_{e_n} and E_{e_m} denotes the QW energies of the electrons and heavy holes as difference from the conduction or valence band, respectively, $E^B_{e_n, hh_m}$ denotes the exciton binding energy and $\Theta(E)$ is the step function. For the simulation model, the δ-distribution, was modified by a Gaussian broadening term to represent the inhomogeneous broadening caused by thermal effects as well as the deviation from ideality of the QW due to the limitations of the growth. The factor $\mathrm{B} = \pi q^2 / (n_r c m_0 \mathrm{h})$ is a material dependent constant. The matrix element contains the electron wave function ψ_{e_n} for the *n*th electron level and the heavy hole wave function ψ_{hh_m} of the *m*th heavy hole level and E_p is the Kane matrix element (~23eV). The first term inside square bracket represents the occupation probability and determines the absorption edge of a bound state where m^*_{e-hh} is the reduced mass of the *e-hh* system, and the second term the additional absorption peak contributed by the excitons. Here a_{ex} denotes the effective Bohr radius of the exciton. For *e-lh* transition a similar expression is obtained with *hh* replaced by *lh* and E_p by $E_p/3$. The absorption of the QWs was calculated using the above formula. The other parameters have been previously stated. On the other hand, the exciton binding energies were analytically evaluated in the framework of fractional–dimensional space [13].

Figure 5 shows modeled and experimental quantum efficiency (*QE*) versus wavelength for qt1897b sample from the Quantum photovoltaics Group of Imperial College. The cell is a p-i-n diode with an i-region containing five QWs that are 9.6 nm wide of compressively strained $In_{0.16}Ga_{0.84}As$ inserted into tensile-strained $GaAs_{0.91}P_{0.09}$ barriers at strain-balance condition. The extra absorption is displayed in the inset of figure 4, at wavelengths in excess of the GaAs band gap where the increase in quantum efficiency in the 880 nm-1μm is readily apparent. The figure also shows the computed *QE* spectrum with DBR, using $r_A = 0.1$ and $r_B = 0.95$. The main feature of this plot is that for a highly reflecting mirror, nearly all photons absorbed contribute to the QE.

This is clearly a desirable feature as it implies that carrier collection from the MQW is very efficient allowing the increase in short circuit current. It is a good indicator that the *QE* of an MQW cell could well approach that of a bulk cell with a similar band-gap if the light could be confined inside the cell until it was completely absorbed.

IV. Influence of anisotropic radiative emission and photon recycling on the SB-QWSC performance

The conventional current-voltage characteristic for a p-i-n solar cell can be written as a function of applied voltage (V) by the well-known Shockley equation for ideal diode to which the generation and recombination currents in the intrinsic region of photogenerated carriers are added. To calculate the recombination current density and photocurrent, anisotropic radiative emission and photon recycling were taken into account. Once the expressions for the effective density of states, the absorption coefficient, the radiative recombination current density, and photocurrent were found for SB-QWSC, then it is possibly to compute the J-V characteristic, and conversion efficiency (η) can be evaluated [3, 14].

The dependence of conversion efficiency on back mirror reflectivity and quantum well number (N_w) is examined in figure 6. This plot suggests that with the addition of a distributed Bragg reflector in the device, fewer quantum wells are required to grow in the i-region in order to achieve high performance. In fact, low energy photons from the radiative recombination in the QWs can be reflected back into i-region and reabsorbed, lowering the radiative recombination current and improving the open-circuit voltage. On the other hand, with increasing N_w it is necessary to use DBR with high reflectivity to overcome the recombination losses.

It can be expected that SB QWSC under concentration will be operating in a regime where recombination is dominated by radiative processes. Therefore, photon recycling effect is favored under solar concentration when photons emitted from radiative recombination are subsequently re-absorbed by the solar cell. This outcome can be observed as an increase in minority carrier lifetime or reduction in dark-current [15].This behavior is shown in Figure 7, where we have examined the conversion efficiency as a function of solar concentration for optimized $GaAs_{0.96}P_{0.04}/In_{0.03}Ga_{0.97}As/GaAs$ solar cell with 20 nm quantum well width [3]. We used $r_A = 0.1$, $r_B = 0.95$ and resistive effects were neglected. It can be observed how the conversion efficiency should increase with solar concentration up to 1000 suns. In any concentration range, the DBR cell efficiency improvement over the non-DBR cell which is explained by the fact of the lower dark current in the DBR cell. This effect also causes that the net increase in conversion efficiency is lower with increasing N_w, as it can be noted in figure 7.

Summary

We have studied the emission light polarized in the plane perpendicular to the quantum well, which is related to the light hole transition and, the emission polarized in the plane of the quantum wells. It was found that the spontaneous emission rates TM and TE increase when the quantum wells are deeper. We have demonstrated that biaxial compressive strain does not suppresses a mode of radiative recombination in the plane of the QWs. The assumption that the photogenerated carriers can escape from the QWs with near unity efficiency, via a thermally-assisted tunneling process, is strongly supported by the several orders difference between gain and radiative recombination. For the modeled SB-QWSC with deeper QWs, both conversion efficiency and open-circuit voltage always fall because the radiative recombination increases.

We have also demonstrated that photon recycling effect have a substantial impact on the overall performance of a SB-QWSC. DBR reflectivity values depend on the number of quantum wells in the i-region. We have optimized SB-QWSC design to achieve single junction efficiencies above 30%. These results on DBR SB-QWSC's show that they hold much promise for use in both single junction and multi-junction space solar cells or terrestrial concentrator solar cells.

References

[1] D.C. Johnson, I. Ballard, K.W.J. Barnham, M. Mazzer, T.N.D. Tibbits, J. Roberts, G. Hill, and C. Calder, in: Proceedings of the 4th World Conference on Photovoltaic Energy Conversion, Hawaii, 7–12 May 2006 (IEEE, 2006), pp. 26–31.

[2] N.J. Ekins-Daukes, J.M. Barnes, K.W.J. Barnham, J.P. Connolly, M. Mazzer, J.C. Clark, R. Grey, G. Hill, M.A. Pate, and J.S. Roberts: Sol. Energy Mater. Sol. Cells Vol. 68 (2001), p.71.

[3] C.I. Cabrera, J.C. Rimada, J.P. Connolly and L. Hernández: J. Appl. Phys. Vol. 113 (2013), 024512.

[4] J.G.J. Adams, B.C. Browne, I.M. Ballard, J.P. Connolly, N.L A. Chan, A. Ioannides, W. Elder, P.N. Stavrinou, K.W.J. Barnham and N.J. Ekins-Daukes: *Recent results for single junction and tandem quantum well solar cells*. Presented at 25th European Photovoltaic Solar Energy Conference and 5th World Conference on Photovoltaic Energy Conversion, Spain, 2010.

[5] J.G.J. Adams, W. Elder, P.N. Stavrinou, J.S. Roberts, M. Gonzalez, J.G. Tischler, R.J. Walters, J. Abell, I. Vurgaftman, J. Meyer, P. Jenkins, K.W.J. Barnham, N.J. Ekins-Daukes: *Experimental measurement of restricted radiative emission in quantum well solar cells*. Proceedings of the 35th IEEE Photovoltaic Specialists' Conference, 2010.

[6] D. C. Johnson, I. M. Ballard, K. W. J. Barnham, J. P. Connolly, and M. Mazzer. Observation of photon recycling in strain-balanced quantum well solar cells. Applied Physics Letters, **90**, 213505, 2007.

[7] J. Singh: *Electronic and Optoelectronic Properties of Semiconductor Structures* (Cambridge University Press, 2003).

[8] ASTM G173-03: Standard Tables for Reference Solar Spectral Irradiances: Direct Normal and Hemispherical on 37 C Tilted Surface, ASTM International. For referenced ASTM standards, visit the ASTM website www.astm.orgi, or contact ASTM Customer Service at service@astm.org.

[9] E. Tsui, J. Nelson, K.W.J. Barnham, C. Button, and J.S. Roberts: J. Appl. Phys. Vol. 80 (1996), p.4599.

[10] H. J. Hovel, Semiconductors and Semimetals, Solar Cells, edited by R. K. Willardson (Academic, 1975), Vol. 11.

[11] J. C. Rimada, L. Hernandez, K. W. J. Barnham, and J. P. Connolly, Phys. Status Solidi B 242(9), 1842–1845 (2005).

[12] G. Bastard, Wave Mechanics Applied to Semiconductor Heterostructures (Editions de Physique, Paris, France, 1988).

[13] H. Mathieu, P. Lefebre, and P. Christol, Phys. Rev. B 46(1), 4092–4101(1992).

[14] M. Courel, J.C. Rimada, L. Hernández: J. Appl. Phys. Vol. 112 (2012), p. 054511.
[15] D.C. Johnson, I. Ballard, K.W.J. Barnham, D.B. Bishnell,J.P. Connolly, M.C. Lynch, T.N.D. Tibbits,N.J. Ekins-Daukes, M. Mazzer, R. Airey, G. Hill, J.S. Roberts. Solar Energy Materials & Solar Cells 87 (2005) 169–179

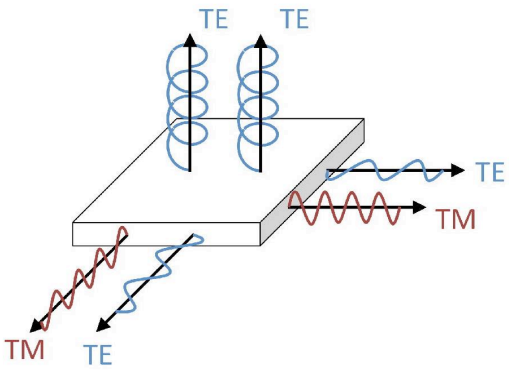

Figure 1

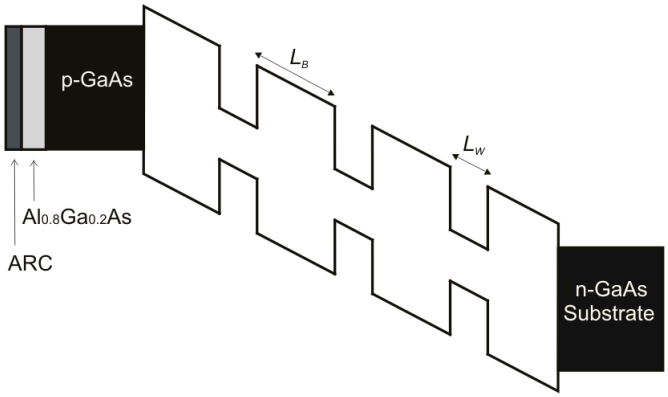

Figure 2

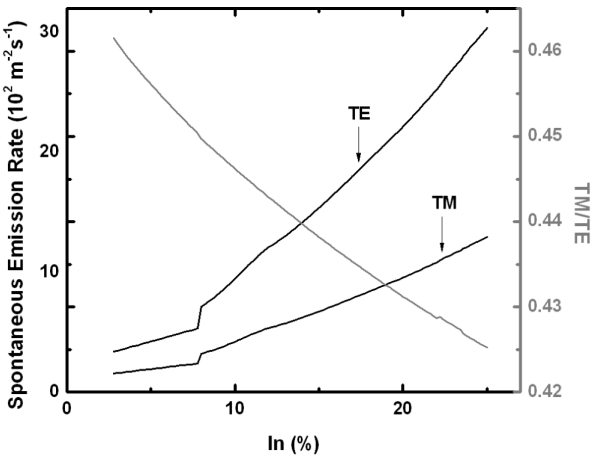
Spontaneous Emission Rate (10^2 $m^{-2}s^{-1}$)
30
20
10
0
0
10
20
In (%)
TE
TM
0.46
0.45
0.44
0.43
0.42
TM/TE

Figure 3

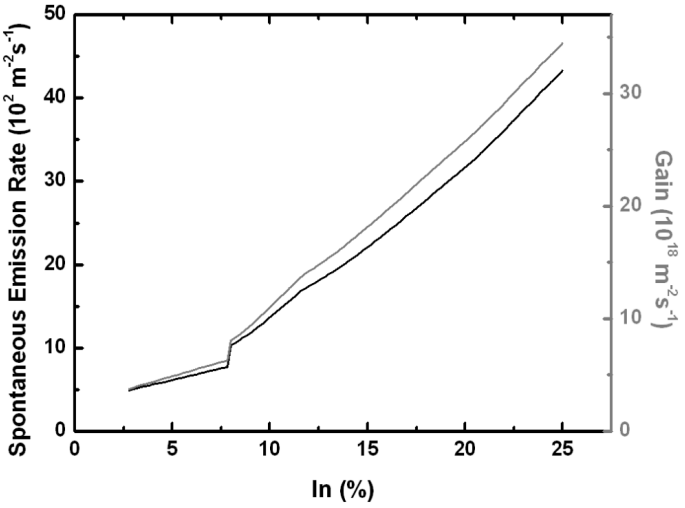
Spontaneous Emission Rate (10^2 $m^{-2}s^{-1}$)
Gain (10^{18} $m^{-2}s^{-1}$)
In (%)
0
10
20
30
40
50
0
5
10
15
20
25
30

Figure 4

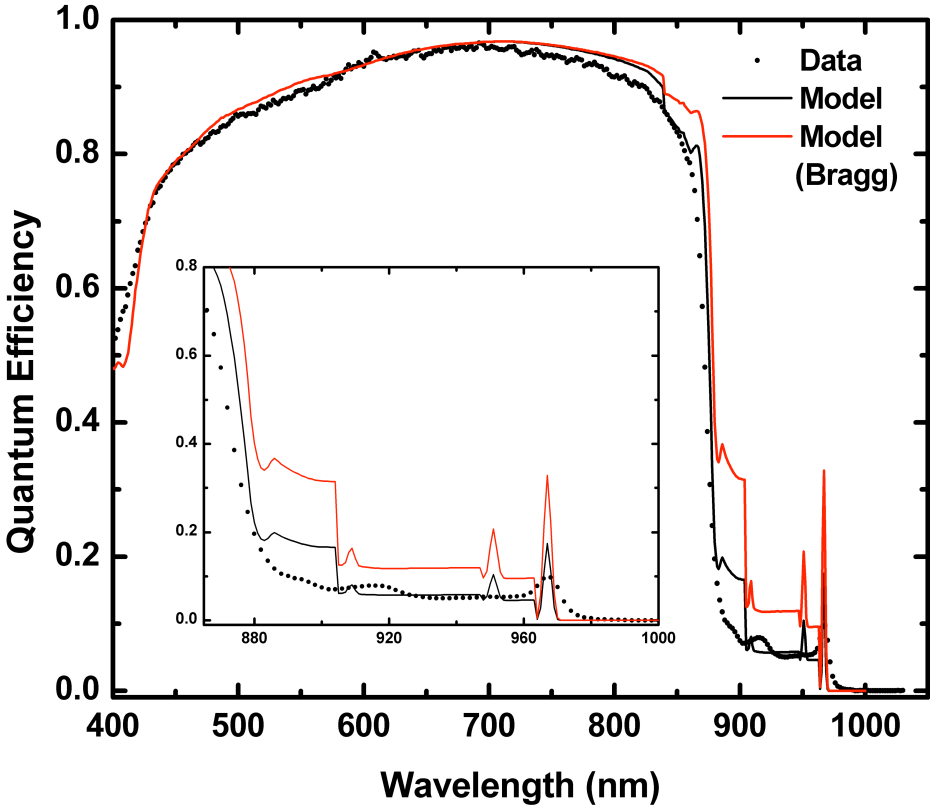
Quantum Efficiency
Wavelength (nm)
Data
Model
Model
(Bragg)
1.0
0.8
0.6
0.4
0.2
0.0
400
500
600
700
800
900
1000
880
920
960
1000

Figure 5

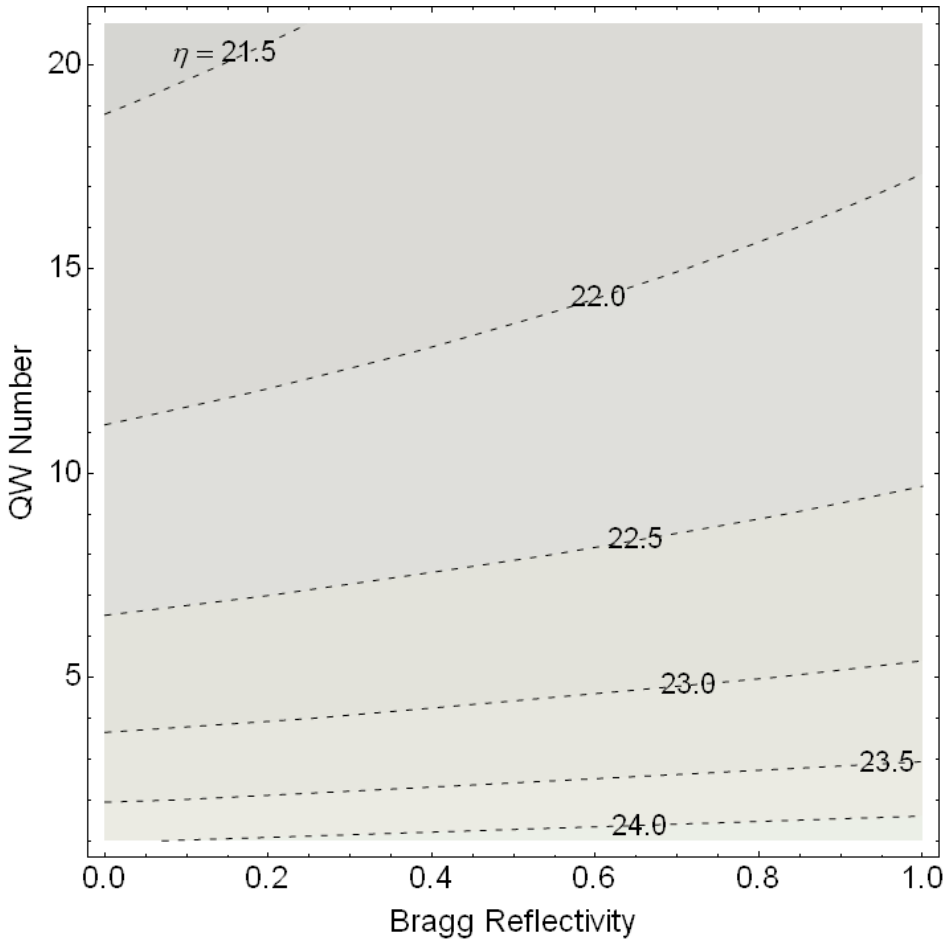
η = 21.5
22.0
22.5
23.0
23.5
24.0
QW Number
20
15
10
5
0.0
0.2
0.4
0.6
0.8
1.0
Bragg Reflectivity

Figure 6

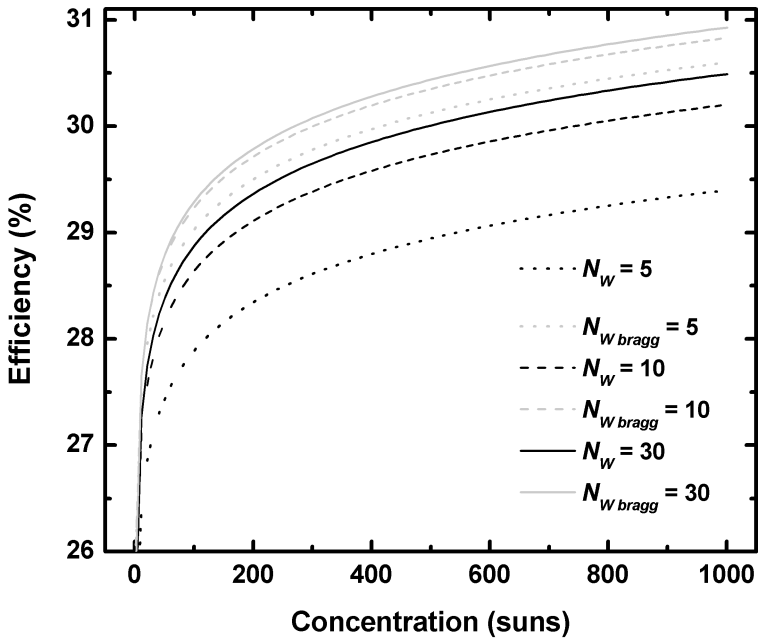
Efficiency (%)
31
30
29
28
27
26
0
200
400
600
800
1000
Concentration (suns)
N_W = 5
$N_{W\,bragg}$ = 5
N_W = 10
$N_{W\,bragg}$ = 10
N_W = 30
$N_{W\,bragg}$ = 30

Figure 7

Figure captions

Fig.1. The polarization of the emission out of the faces and edges of a quantum well. Light polarized in the TM mode can only be emitted out of the edge. Light polarized in the TE mode can be emitted out of the face or the edge [4, 5].

Fig.2 The schematic band-structure of the SB-QWSC. The QW stack is embedded within the depletion zone of the GaAs cell and extends the absorption edge of the cell beyond that of a classical GaAs solar cell.

Fig. 3. Modeled spontaneous emission rate for TE and TM modes and TM/TE ratio versus In composition for 10 well embedded within i-region of the SB-QWSC. Well width, L_W=15 nm and P composition, y =0.05. The TE mode is favored over TM mode, but both polarized emissions increase with well depth.

Fig. 4. Spontaneous emission rate and gain versus In composition for 10 well embedded within intrinsic region of the SB-QWSC. Well width, L_W=15 nm and P composition, y =0.05. Gain is several orders greater than radiative recombination.

Fig. 5. Modelled and experimental quantum efficiency versus wavelength for 5 well qt1897b sample from the Quantum photovoltaics Group of Imperial College. The inset shows the wavelength range dominated by the QW absorption with and without influence of Bragg reflector.

Fig. 6. Contour plot for conversion efficiency as a function of Bragg reflectivity and quantum well number. P composition, y = 0.09. In composition, x=0.17 and L_W=9.6 nm.

Fig. 7. Conversion efficiency as a function of solar concentration for several $GaAs_{0.96}P_{0.04}/In_{0.03}Ga_{0.97}As/GaAs$ SB-QWSC which differ in the number of QW embedded within the i-region with and without influence of Bragg reflector.